TABLE OF CONTENTS

NASA Contractor Report 3310

The Buckling Analysis of Imperfection Sensitive Shell Structures

Johann Arbocz and Charles D. Babcock, Jr.

GRANT NSG-1005
AUGUST 1980

NASA

NASA Contractor Report 3310

The Buckling Analysis of Imperfection Sensitive Shell Structures

Johann Arbocz and Charles D. Babcock, Jr.
California Institute of Technology
Pasadena, California

Prepared for
Langley Research Center
under Grant NSG-1005

NASA
National Aeronautics
and Space Administration

Scientific and Technical
Information Branch

1980

Blank Page

TABLE OF CONTENTS

I. INTRODUCTION

The design of buckling critical shell structures is complicated by the presence of geometric imperfections inherent in any manufacturing process. These small deviations from the perfect geometry are largely responsible for the sizeable discrepancy between analysis and test results for many shell buckling problems. The usual method of incorporating these initial imperfections into the design process is to use an empirically determined "knockdown" or correlation factor (ref. 1). Recently developed geometrically nonlinear structural analysis computer codes (for example, ref. 2) have made it possible to calculate the effect on buckling of an assumed imperfection. However, the economical use of such tools requires considerable knowledge on the part of the user as to the physical behavior of the imperfect shell structure. This knowledge can be gained using a hierarchy of imperfection sensitivity analyses developed over recent years.

This report describes in detail a study on one well characterized stringer stiffened cylindrical shell. The initial imperfections and prebuckling growth under axial load were measured as well as the axial buckling load. The results of various analyses for imperfect shells are presented and compared to each other and to test results. Finally, a procedure to calculate a "knockdown factor" is proposed. This procedure, based upon a known or expected design imperfection makes optimal use of state-of-the-art analysis capability.

The work reported in this paper was carried out at the California Institute of Technology under Research Grant NSG-1005 from the National Aeronautics and Space Administration. Some of the computations were carried out at the Delft University of Technology Computing Center after the first author's move to the Netherlands. The support of both of these institutions is gratefully acknowledged.

The authors also wish to express their appreciation to Dr. Kiam Oey, the GALCIT staff and Mr. Kees Venselaar for their assistance in carrying out this work and in the preparation of this report.

LIST OF SYMBOLS

A_1	cross-sectional area of stringer
b	imperfection sensitivity factor
d_1	stringer spacing
e_1	distance between centroid of stringer cross-section and middle surface of skin
E	Young's modulus
I_{11}	moment of inertia of stringer cross-section about its centroidal axis
I_{t_1}	torsional modulus of the stringer cross-section
i,k	number of half waves in the axial direction
ℓ	number of full waves in the circumferential direction
L	shell length
N_x	axial stress resultant
q,r,s	imperfection model parameters
R	shell radius
t	shell thickness
u,v,w	axial, circumferential and radial displacement components
$\bar{w}$	imperfection in radial direction
$w,_x$	$\frac{\partial w}{\partial x}$
$\bar{X}_A,\bar{X}$	imperfection model parameters
x,y	axial and circumferential coordinates of the shell
$\bar{\delta}$	imperfection in lowest buckling mode
η	calculated buckling load divided by experimental buckling load
θ	circumferential coordinate, $\theta = y/R$
ν	Poisson's ratio
$\xi_{io},\xi_{k\ell}$	initial imperfection amplitudes
ρ	nondimensional loading parameter
$\phi_{k\ell}$	initial imperfection circumferential phase shift

Subscripts

cal	calculated
exp	experimental

II. CHARACTERIZATION OF THE TEST SHELL

The cylindrical shell studied in this report is the aluminum test shell designated as AS-2 in ref. 3. The shell is axially stiffened with integral rectangular stiffeners. The shell properties are given in Table I. The shell was buckled under axial compression and its initial imperfection and prebuckling growth were measured. The measurement device and testing machine are shown in fig. 1, with a shell similar to the one under study in the testing machine. The stiffener geometry and the test configuration are described in fig. 2. The shell buckled at an axial load of 226.3 N/cm.

Before the shell was buckled the shell's initial imperfection was measured and is shown in fig. 3. This figure shows the best fit initial imperfection (ref. 4). The imperfection has been normalized by the shell thickness and is rolled out to show the circumferential and axial distribution. During the loading process the shell surface shape is remeasured and the initial imperfection is subtracted from that measurement. This gives the prebuckling deformation. A typical result at a load close to the buckling load is shown in fig. 4. The characteristic wave form has nine circumferential waves and one axial half wave.

The perfect shell was analyzed using shell of revolution computer codes SRA (ref. 5) and BOSOR (ref. 6). The shell loading device and actual shell was modeled in order to determine the influence of the experimental boundary conditions. The prebuckling deformation (axisymmetric) is shown in fig. 5. It is seen that the load cell does not appear to present a fully clamped boundary condition. The buckling mode for this case is also shown in fig. 5. The value calculated for the critical load with the experimental boundary conditions is 316.6 N/cm (180.8 lb/in.). However, this value is approximately 0.1% lower than that obtained using the fully clamped conditions (ref. 7). Therefore it seems reasonable to assume the fully clamped conditions in further analyses.

The analysis described above considers the influence of the prebuckling deformation due to the end constraints. A simplified version of the problem considers only a membrane prebuckling stress and gives the following results

$$N_x = 320.8 \text{ N/cm } (183.2 \text{ lb/in}).$$

This is only slightly above the buckling load including the edge effect. The membrane stress state will be assumed in further calculations for the perfect shell. The various buckling loads are summarized below.

Conditions	Load N/cm	Load lb/in.
Analysis		
Experimental Set-up	316.6	180.8
Fully Clamped-Nonlinear Bending Prebuckling	316.8	180.9
Fully Clamped-Membrane Prebuckling	320.8	183.2
Experiment	226.3	129.2

In studying the behavior of the imperfect shell it is necessary to determine the buckling modes of the perfect shell corresponding to the lowest few buckling loads. An eigenvalue map of modes calculated using membrane prebuckling and fully clamped boundary conditions is shown in fig. 6. The figure identifies by circumferential wave number and order of eigenvalue those modes that have buckling loads close to the lowest one. There are approximately 14 modes that correspond to loads less than 10% above the lowest eigenvalue. From previous work it is known that the imperfections in these modes are the ones which most influence the imperfect shell behavior. The values of the buckling loads are given in Table 2 for a few of the lowest loads. These results were obtained using the BOSOR computer code and are slightly higher than similar results using the SRA computer code. The mode shapes of the first four modes with 14 circumferential waves are shown in fig. 7. As can be seen a simple counting of nodes is not sufficient to identify a mode as can be done for simply supported boundary conditions.

The next item that must be examined is the character of the initial imperfection. Expanding the imperfection in a double Fourier expansion has been a useful tool in previous studies (ref. 7). The expansion used depends upon the application but in the subsequent analysis it will be useful to have the axisymmetric imperfection as a cosine expansion and the asymmetric imperfection as a sine expansion

$$\bar{w}(x,y)/t = \sum_{i=0}^{N} \xi_{i0} \cos \frac{i\pi x}{L} + \sum_{k,\ell=1}^{M\ N} \xi_{k\ell} \sin \frac{k\pi x}{L} \cos \left(\frac{\ell y}{R} + \phi_{k\ell}\right).$$

The coefficients $\xi_{k\ell}$ are shown in fig. 8 for the first few harmonics. If these coefficients are displayed on a log-log basis (ref. 8) a reasonable approximation to straight lines is observed (neglecting the $\ell = 1$ mode). This allows the fitting (by a least square technique) of the following imperfection model (ref. 7).

$$\xi_{i0} = \frac{\bar{X}_A}{i^q} \quad , \quad \xi_{k\ell} = \frac{\bar{X}}{k^r \ell^s}$$

This imperfection model will be used in subsequent analyses rather than the measured amplitudes. The imperfection model parameters were obtained in two different manners. First a group of three similar shells (including AS-2) were fit by a common imperfection model (ref. 7). Next, the imperfection of shell AS-2 alone was fit. The results are given below

	Group of 3 Shells	AS-2
$\bar{X}_A$	.0072	--
$\bar{X}$	1.1973	1.1016
q	.027	--
r	1.123	1.103
s	1.227	1.359

The results show that both methods give similar coefficients for the imperfection model.

III. ANALYSIS OF THE IMPERFECT SHELL

The buckling analysis of an imperfect shell can be carried out in a variety of ways with varying degrees of complexity. The purpose of this section is to determine the success of these types of analyses in predicting the buckling load of the test shell described in section II. An additional purpose is to discover what each analysis has to contribute to the next level of analysis complexity.

The simplest type of imperfection sensitivity analysis is that introduced by Koiter (ref. 9) and further developed by Budiansky and Hutchinson (refs. 10 and 11). In this analysis the sensitivity of the buckling load to the imperfection having the shape of the buckling mode is studied. This analysis was specialized to stiffened cylindrical shells by Hutchinson and Amazigo (ref. 12) for the case of classical simple support boundary conditions. These results are expressed as

$$(1 - \rho)^{3/2} = \frac{3}{2} \sqrt{-3b}\ \rho\ |\bar{\delta}|$$

where $|\bar{\delta}|$ is the imperfection in the lowest buckling mode, b is the imperfection sensitivity factor, and ρ is the ratio of imperfect shell buckling load to the perfect shell buckling load. For the shell being studied, 10 full circumferential waves and one axial half wave for simple support boundary conditions, corresponds to $|\bar{\delta}| = 0.054$, $b = -0.0308$. Using the above parameters the imperfect shell buckling load can be calculated to be

$$\rho = 0.92$$

This load is considerably higher than the experimental load ($\rho = 0.71$). It therefore appears necessary to include additional terms in the imperfection when calculating the imperfect shell buckling load.

The next level of complexity in the analysis is to consider additional modes of imperfections. This will be referred to as the Multimode Analysis (refs. 7, 13, and 14). The nonlinear shell equations are solved by expanding the imperfection and radial displacement in a Fourier series and then solving

the compatibility equation. A Galerkin procedure is then used to reduce the problem to a set of nonlinear algebraic equations that are solved numerically. The expansion for the displacement is the same as previously introduced for the initial imperfection.

The main problem in using the Multimode Analysis is the proper selection of the deflection modes. The imperfection in these modes must be of a significant magnitude and these modes must also correspond to buckling loads close to the lowest load. It has also been found that special attention must be given to the satisfaction of the axial and circumferential coupling conditions. It has been shown (ref. 15) that for the degenerate case of one axisymmetric $(i,0)$ and one asymmetric mode (k,ℓ) there is a single coupling relation $i = 2k$. Furthermore, it has been found that coupling between three asymmetric modes with wave-numbers (k_1,ℓ_1), (k_2,ℓ_2) and (k_3,ℓ_3) will occur if the relations $k_1 + k_2 + k_3$ = an odd integer and $\ell_3 = |\ell_1 \pm \ell_2|$ hold. This implies that if the coupling conditions are satisfied, then the resulting buckling load of the shell will be lower than the buckling load which is predicted with each mode considered separately.

It is also important to choose modes that have low buckling loads. The eigenvalue map, as introduced earlier for the fully clamped boundary conditions, helps in the proper selection. For simply support boundary conditions the results are shown in fig. 9. There are only three buckling loads within 10% of the lowest one.

The simplest multimode selection uses the (1,10) mode from the eigenvalue map and the coupled mode (2,0). This results in a buckling load of

$$\rho = 0.904 \ .$$

This is slightly lower than that obtained from the Koiter type analysis. To include the other important modes having low buckling loads, coupling modes must be added to provide the interaction (ref. 13). The resultant 7-mode solution produces a buckling load of

$$\rho = 0.825 \ .$$

The inclusion of 7 more modes does not produce a significantly lower buckling load (see Table 3).

The next level of complexity in analysis is to use a two dimensional nonlinear shell analysis such as STAGS (ref. 2). With the use of this type of numerical tool, one can, in principle, determine the buckling load of a complete shell structure including the effect of an arbitrary prescribed initial imperfection. In practice, the cost of performing such an analysis dictates that the problem size be cut down usually by modeling only a portion of the shell structure. This approach will be used for this analysis. The shell model used a 180° segment with symmetry conditions imposed at 0° and 180° as well as at the shell mid-length. The mesh used was 21 by 131 points in the axial and circumferential directions respectively. This mesh was chosen based upon a convergence study (ref. 16).

The first STAGS imperfection analysis uses a 7-mode imperfection model which is the same as the Multimode Analysis 7-mode case (Table 3). The imperfection is

$$\bar{w}/t = 0.0061 \cos\left(\frac{2\pi x}{L}\right) - \sin\frac{\pi x}{L}\left\{0.5072 \cos\left(2\frac{y}{R}\right)\right.$$

$$+ 0.0801 \cos\left(9\frac{y}{R}\right) + 0.0704 \cos\left(10\frac{y}{R}\right) + 0.0626 \cos\left(11\frac{y}{R}\right)$$

$$\left. + 0.0320 \cos\left(19\frac{y}{R}\right) + 0.0283 \cos\left(21\frac{y}{R}\right)\right\}$$

The sign of the asymmetric component of the imperfection has been taken as negative so that the imperfection is inwardly directed at $\theta = 0^\circ$ (ref. 16).

The results of the STAGS analysis and the corresponding Multimode Analysis are shown in figures 10, 11 and 12. Figure 10 shows the maximum displacement as a function of the axial load. Here the maximum displacement is the radial displacement w at $x = L/2$ and $\theta = 0^\circ$. The results of the nonlinear STAGS runs are indicated by circles. Above the last point the determinant of the stiffness matrix changes sign indicating the occurrence of an instability. The axial load corresponding to the last converged solution is the collapse load $\rho = 0.829$. The load parameter ρ has been nondimensionalized by 320.8 N/cm, which is the buckling load for the perfect shell AS-2 using

membrane prebuckling and C-4 ($u = v = w, x = w,_x = 0$) boundary conditions. The results of the corresponding Multimode Analysis are given by the solid curve. Its limit point occurs at $\rho = 0.825$, which agrees just about exactly with the value obtained by STAGS. Further, as can be seen from figures 11 and 12, the shapes of the radial displacements at the center of the shell (at $x = L/2$) plotted as a function of the circumferential angle θ are very similar for the two methods. Their amplitudes are, however, different by about a factor of 2. This difference is thought to occur due to the difference in the boundary conditions used in the two analyses. The boundary conditions used with the STAGS analysis were fully clamped while those of the Multimode Analysis more closely approximate simply supported. Despite this difference in displacement, the closeness of the buckling loads tends to confirm the practice of using the simpler Multimode Analysis as a first guess for the imperfect shell buckling load (ref. 7).

The analysis just described provides an interesting comparison between the Multimode Analysis and STAGS. However, the results predicted by STAGS ($\rho = 0.829$) is still considerably higher than the experimental results

$$\rho = 226.3/316.6 = 0.714.$$

It is apparently necessary to include more information about the initial imperfection in the STAGS analysis.

Based upon the eigenvalue map (fig. 6) it was decided to include asymmetric modes with up to four half waves in the axial direction. Symmetry can no longer be used at the shell mid-length since now both symmetric and antisymmetric modes are involved in the response. This necessitates more mesh points along the length. In order to keep the numerical problem manageable, the circumferential segment of the shell model was reduced to 90^o. With symmetry conditions imposed at $\theta = 0^o$ and $\theta = 90^o$ the shell cannot respond to odd numbered circumferential harmonics and these harmonics are eliminated from the imperfection. Even numbered harmonics up to $\ell = 18$ are included. The imperfection for this case is given below:

$$\bar{w}/t = \sum_{i=2}^{8} \xi_{i0} \cos\frac{i\pi x}{L} - \sum_{k=1}^{4} \sum_{\ell=12}^{18} \xi_{k\ell} \sin\frac{k\pi x}{L} \cos\frac{\ell y}{R}$$

$$- \sum_{k=1}^{2} \sum_{\ell=2}^{10} \xi_{k\ell} \sin\frac{k\pi x}{L} \cos\frac{\ell y}{R}\,, \quad \text{even terms in } i,\ell \text{ sums.}$$

The ξ coefficients are given in Table 4. The imperfection described by this 30-mode model is shown in fig. 13. From this figure it can be seen that the elimination of the phase angle ($\phi_{k\ell}$) from the cosine circumferential harmonics biases the imperfection at $\theta = 0^o$, 180^o.

The analysis was carried out using a 40 by 40 mesh. The results for the maximum radial displacement (at $x/L = 0.28$, $\theta = 0^o$) are shown in fig. 14. Each point indicated by a circle represents a STAGS converged solution. Above $\rho = 0.759$ the displacement is increasing very rapidly with load and additional solutions have not been obtained. A good estimate of the collapse load is $\rho = 0.760$. The load parameter ρ has been nondimensionalized by 320.8 N/cm, which is the buckling load for the perfect shell AS-2 using membrane prebuckling and C-4 boundary conditions.

The displacements of the last converged solution are shown in figures 15 and 16. The bias at $\theta = 0^o$ is clear in fig. 15 although a $\theta = 10^o$ harmonic appears to be emerging. The axial variation (fig. 16) shows both a $k = 1$ and $k = 2$ dependence.

The collapse load as calculated by STAGS is estimated to be

$$N_{x_{cal}} = .760 \times 320.8 = 243.8 \text{ N/cm } (139.2 \text{ lb/in.}).$$

The experimental buckling load (ref. 3) is

$$N_{x_{exp}} = 226.3 \text{ N/cm } (129.2 \text{ lb/in.}).$$

The ratio (η) of these two loads is

$$\eta = N_{x_{cal}}/N_{x_{exp}} = 1.08$$

The analyses just described vary greatly in difficulty of execution. The Koiter type asymptotic analysis is the simplest to use but does not adequately predict the influence of the complex imperfection pattern characteristic of shell structures. The Multimode Analysis developed for the cylindrical shells does a fair job of prediction, but the extension of this type of analysis to more general geometry and boundary conditions does not seem warranted in light of presently available shell computer codes. The usefulness of this analysis is that the modal coupling is explicitly displayed and that the importance of imperfection modes can be examined (for the cylindrical geometry) without difficulty. The STAGS analysis can give results for a knockdown factor that are within the accuracy expected for imperfection sensitive buckling problems. However, before this type of tool is used, it is prudent to understand the buckling behavior of the perfect shell structure. A procedure to use STAGS (or similar analysis) in the selection of a knockdown factor (ρ) will be outlined in the next section.

IV. PROPOSED ANALYSIS PROCEDURE

The previous sections have described the analysis and correlation studies carried out for a particular stiffened shell under axial compressive loading. The study of this idealized problem was undertaken with the objective of establishing a rational analysis procedure for the incorporation of geometric imperfections into the design of buckling critical shell structures. The proposed procedure will be outlined as applied to a shell of revolution under axially symmetric loads.

There are three necessary ingredients to the proposed procedure. These are listed below and briefly discussed.

(a) Buckling analysis capability for a shell of revolution under axially symmetric loads. A computer code such as BOSOR (ref. 6) or SRA (ref. 7) will satisfy this requirement.

(b) A geometrically nonlinear shell analysis for a shell of revolution with an asymmetric initial imperfection. The STAGS (ref. 2) computer code will satisfy this requirement.

(c) A design imperfection. At the present time this is the most elusive ingredient. The imperfection model introduced in section II is one approach but has yet to be extended to larger cylindrical shell structures or other shells of revolution.

Using these tools the following steps are to be carried out:

(1) Find the buckling load of the perfect shell structure using the analysis (a). Establish the importance of the type of prebuckling deformation used in the analysis. Determine which part of the complete shell structure is likely to buckle and the appropriate end conditions when modeling only the critical subsection of the complete shell structure.

(2) Using the appropriate subsection of the complete shell and the simplifications justified in Step 1), calculate all buckling loads using analysis (a), within 50% of the lowest buckling load. The associated buckling modes will typically have circumferential wave numbers other than that corresponding to the lowest buckling load.

(3) Using analysis (b) and imperfections corresponding to all modes calculated in 2), find the buckling load of the shell subsection. This step requires the use of the design imperfection (c) which should represent the

manufacturing procedure (and tolerances) to be used when producing the shell structure.

The procedure outlined above is intended to replace the usual empirical knockdown factor. It is anticipated that the conventional approach and the proposed procedure would both be used until adequate experience has been developed by subsequent testing of shell structures designed using this approach. It is not expected that this procedure would replace engineering judgment, only that this judgment would be guided by the rational use of the nonlinear shell analysis capability presently available.

REFERENCES

1. Anonymous, "Buckling of Thin-Walled Cylinders," NASA SP 8007, 1968.
2. Almroth, B. O., and Brogan, F. A., "The STAGS Computer Code," NASA CR-2950, Feb. 1978.
3. Singer, J., Arbocz, J. and Babcock, C. D., "Buckling of Imperfect Stiffened Cylindrical Shells under Axial Compression," AIAA Journal, Vol. 9, No. 1, Jan. 1971, pp. 68-75.
4. Arbocz, J. and Babcock, C. D., "The Effect of General Imperfections on the Buckling of Cylindrical Shells," Journal of Applied Mechanics, Vol. 36, No. 1, March 1969, pp. 28-38.
5. Cohen, G. A., "User Document for Computer Programs for Ring-Stiffened Shells of Revolution," NASA CR-2086, March 1973.
6. Bushnell, D., "Stress, Stability and Vibration of Complex, Branched Shells of Revolution: Analysis and User's Manual for BOSOR-4," NASA CR-2116, Oct. 1972.
7. Arbocz, J. and Babcock, C. D., "Prediction of Buckling Loads Based on Experimentally Measured Initial Imperfections," Proceedings IUTAM Symposium on Buckling of Structures, Springer Verlag, Heidelberg, 1976, pp. 291-311.
8. Babcock, C. D., "Experiments in Shell Buckling," Thin Shell Structures, Theory, Experiment and Design, (Y. C. Fung and E. E. Sechler, eds.), Prentice-Hall, Englewood Cliffs, N. J., 1974.
9. Koiter, W. T., "On the Stability of Elastic Equilibrium," Ph.D. Thesis, in Dutch, Techn. Univ. Delft, Netherlands, H. T. Paris, Amsterdam. English translation issued as NASA TT-F-10, 1967.
10. Budiansky, B., "Theory of Buckling and Post-Buckling Behavior of Elastic Structures," Advances in Applied Mechanics, Vol. 14, Academic Press, pp. 1-65, 1974.
11. Budiansky, B. and Hutchinson, J. W., "Dynamic Buckling of Imperfection Sensitive Structures," Proceedings XI. Intern. Congr. Appl. Mech., Springer Verlag, Berlin, 1964, pp. 636-651.
12. Hutchinson, J. W. and Amazigo, J. C., "Imperfection Sensitivity of Eccentrically Stiffened Cylindrical Shells," AIAA Journal, Vol. 15, No. 3, March 1967, pp. 392-401.

13. Arbocz, J., "The Effect of Initial Imperfections on Shell Stability," Thin Shell Structures, Theory, Experiment and Design. (Y. C. Fung and E. E. Sechler, eds.), Prentice-Hall, Englewood Cliffs, N. J., 1974.

14. Thurston, G. A. and Freeland, M. A., "Buckling of Imperfect Cylinders under Axial Compression," NASA CR-541, July 1966.

15. Arbocz, J. and Babcock, C. D., "A Multi-Mode Analysis for Calculating Buckling Loads of Imperfect Cylindrical Shells," GALCIT Report SM 74-4, California Institute of Technology, Pasadena, June 1974.

16. Arbocz, J., and Babcock, C. D., "Utilization of STAGS to Determine Knock-down Factor from Measured Imperfections," Delft University of Technology Report, LR-275, Nov. 1978.

Table 1.- Geometric and material properties of shell AS-2.

$t = 1.96 \times 10^{-2}$ cm	(0.00774	in.)
$L = 13.97$ cm	(5.50	in.)
$R = 10.16$ cm	(4.00	in.)
$d_1 = 8.034 \times 10^{-1}$ cm	(0.3163	in.)
$e_1 = 3.368 \times 10^{-2}$ cm	(0.01326	in.)
$A_1 = 7.987 \times 10^{-3}$ cm^2	(0.1238×10^{-2}	in.^{2})
$I_{11} = 1.504 \times 10^{-6}$ cm^4	(0.3613×10^{-7}	in.^{4})
$I_{t_1} = 4.945 \times 10^{-6}$ cm^4	(0.1188×10^{-6}	in.^{4})
$E = 6.895 \times 10^6$ N/cm^2	(10×10^6	psi)

$\nu = 0.3$ $\quad L/R = 1.375$

$R/t = 517$

Table 2.- Buckling loads (N/cm) for shell AS-2 using memb ane prebuckling and clamped boundary conditions ($u = v = w = w_{,x} = 0$).

Eigenvalue \ Circumferential Wave Number, ℓ	10	11	12	13	14	15	16	17	18	19	20
1	393.8	357.2	341.3	331.8	322.7	323.2	330.7	342.4	354.1	370.0	387.9
2	445.9	389.8	353.2	335.7	333.1	332.4	335.2	342.5	356.1	371.0	389.0
3	493.9	464.1	435.4	418.7	406.6	399.3	399.4	406.8	415.2	425.5	441.0
4	494.0	469.8	441.6	420.9	410.6	407.1	406.5	409.0	419.5	434.0	448.2
5	503.5	482.8	472.3	465.9	460.4	458.3	460.5	468.3	484.0	495.8	506.6
6	506.2	486.1	474.5	467.8	468.7	471.9	475.8	480.8	487.3	507.0	529.8
7	530.3	518.8	515.6	520.8	521.6	524.1	528.7	535.8	546.8	565.9	599.2
8	537.0	526.8	522.6	521.0	534.5	549.1	560.0	569.3	578.5	588.4	599.8

Table 3.- Buckling loads calculated by the Multimode Analysis.

No. of modes	ρ
2-modes (2,0) + (1,10)	0.904
4-modes (2,0) + (1,10) + (9,10) + (10,0)	0.903
7-modes (2,0) + (1,2) + (1,9) + (1,10) + (1,11) + (1,19) + (1,21)	0.825
14-modes (2,0) + (1,2) + (1,9) + (1,10) + (1,11) + (1,19) + (1,21) + (9,2) + (9,9) + (9,10) + (9,11) + (9,19) + (9,21) + (10,0)	0.824

Table 4.- The 30-mode imperfection model.

Mode no.	k,i	ℓ	$\xi_{k\ell}$	Mode no.	k,i	ℓ	$\xi_{k\ell}$
1	2	0	0.00461	16	3	18	-0.00645
2	4	0	0.00363	17	4	12	-0.00816
3	6	0	-0.00032	18	4	14	-0.00661
4	8	0	-0.00200	19	4	16	-0.00552
5	1	12	-0.03761	20	4	18	-0.00470
6	1	14	-0.03050	21	1	2	-0.42945
7	1	16	-0.02544	22	1	4	-0.16741
8	1	18	-0.02168	23	1	6	-0.09649
9	2	12	-0.01751	24	1	8	-0.06526
10	2	14	-0.01420	25	1	10	-0.04819
11	2	16	-0.01185	26	2	2	-0.19998
12	2	18	-0.01009	27	2	4	-0.07796
13	3	12	-0.01120	28	2	6	-0.04493
14	3	14	-0.00908	29	2	8	-0.03039
15	3	16	-0.00758	30	2	10	-0.02244

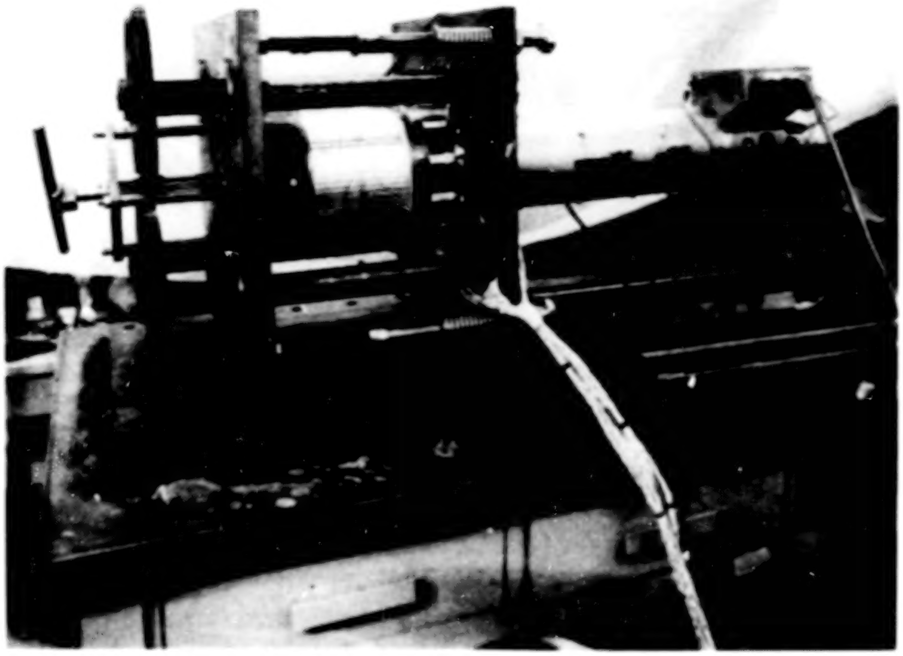

Fig.1 Testing machine with stringer-stiffened shell.

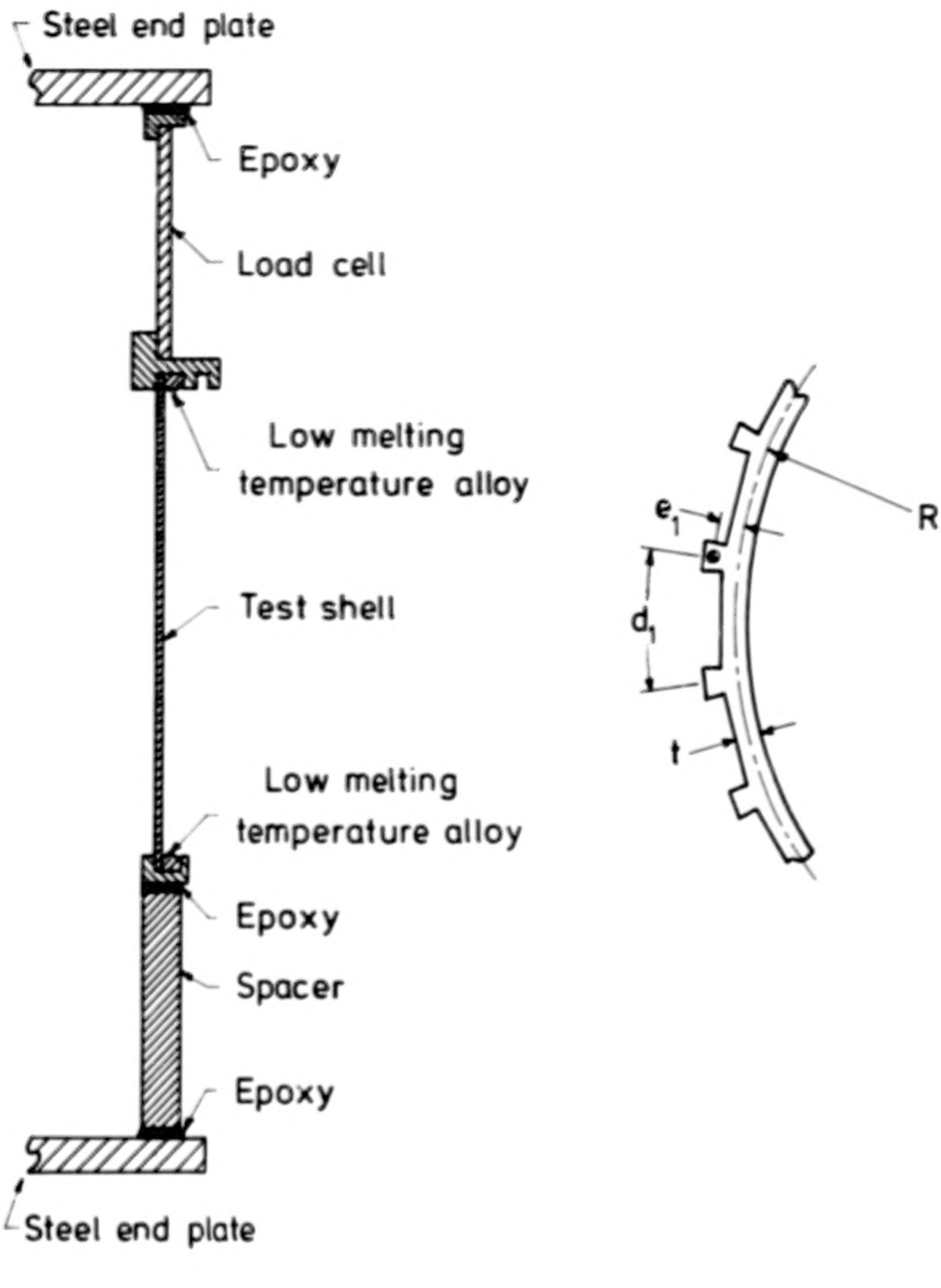

Fig.2 Stiffened shell geometry and test configuration.

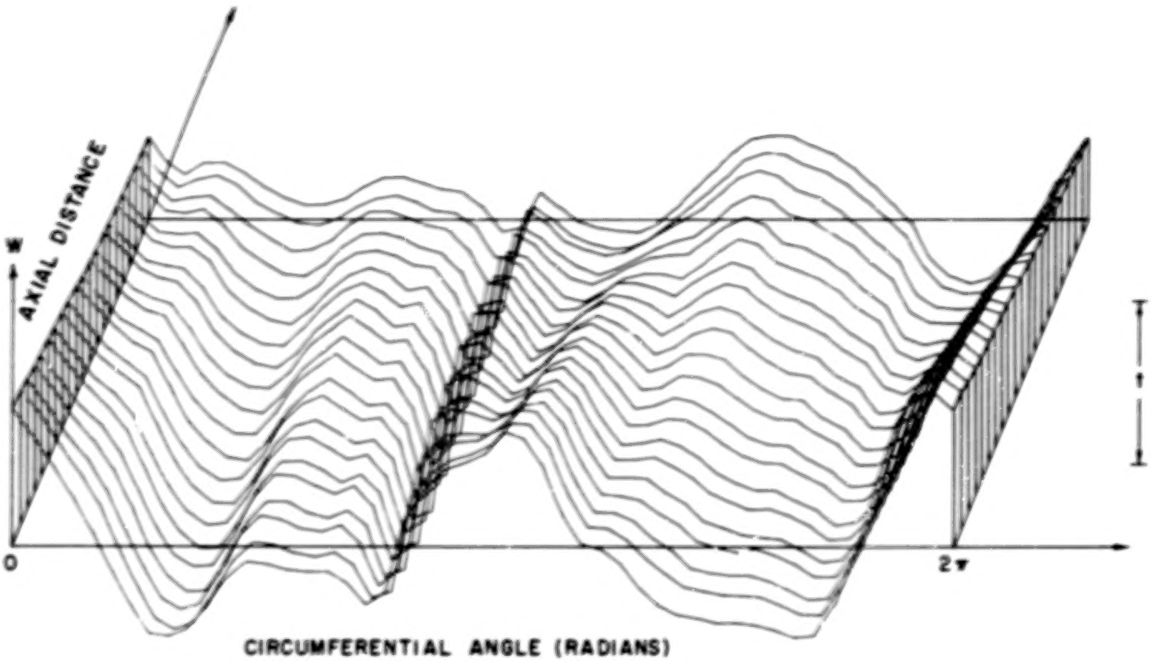

Fig.3 Measured initial shape of the stringer stiffened shell AS-2.

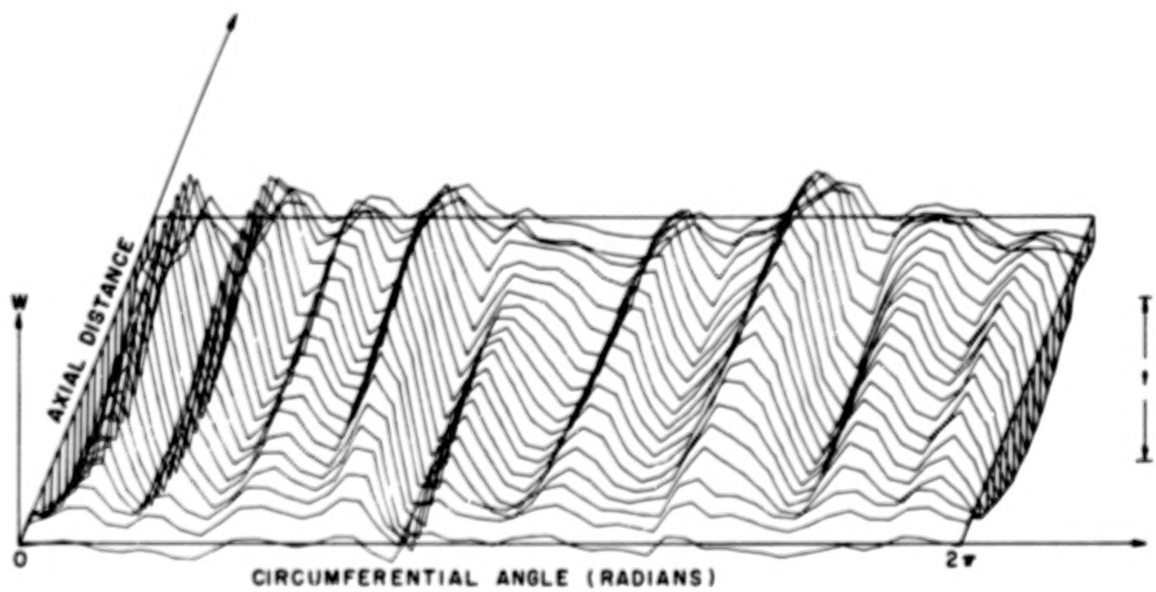

Fig.4 Measured prebuckling growth of the stringer stiffened shell AS-2 at $\rho = 0.629$.

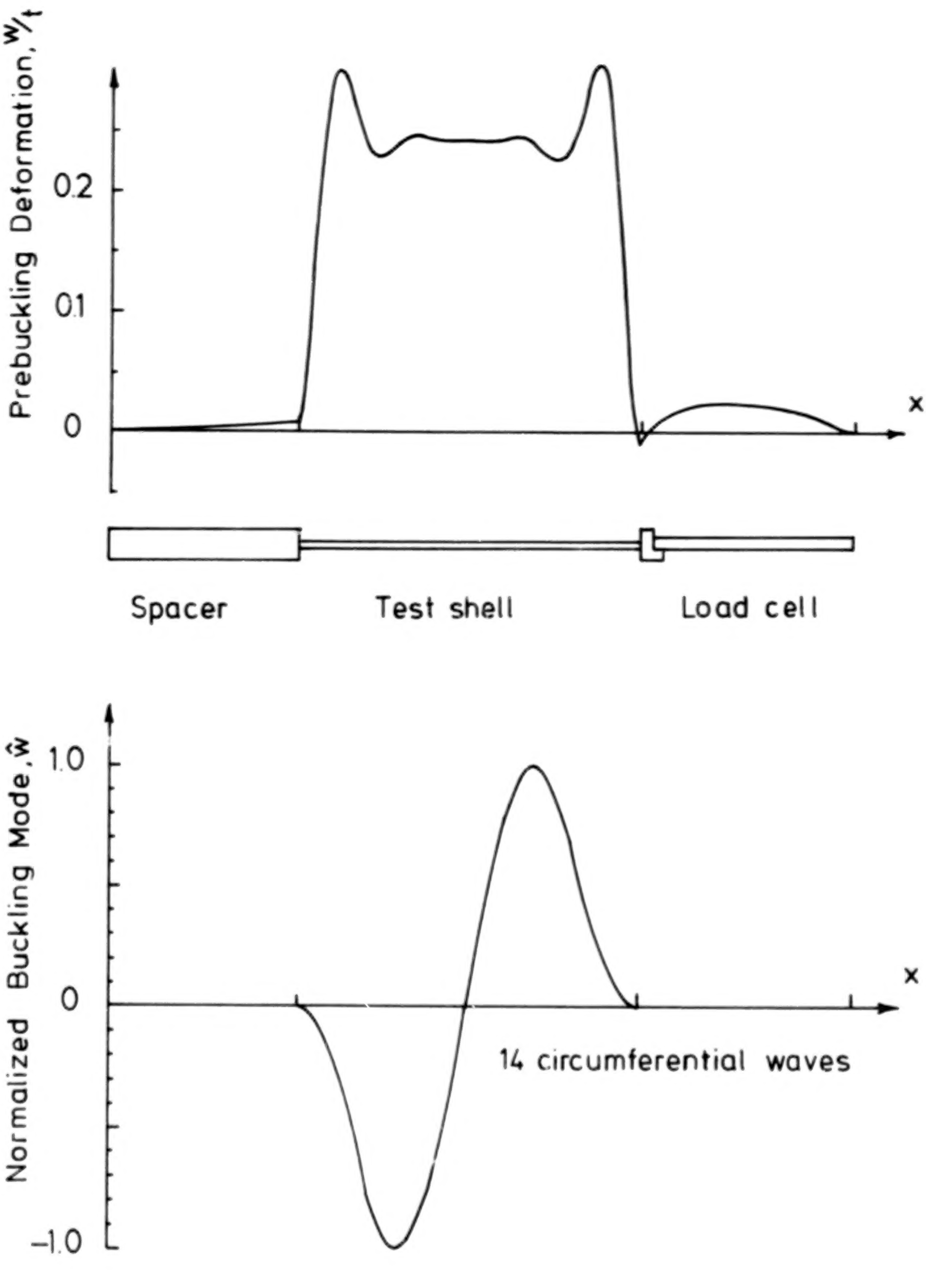

Fig.5 Prebuckling deformation and buckling mode for shell AS-2 (Experimental boundary conditions).

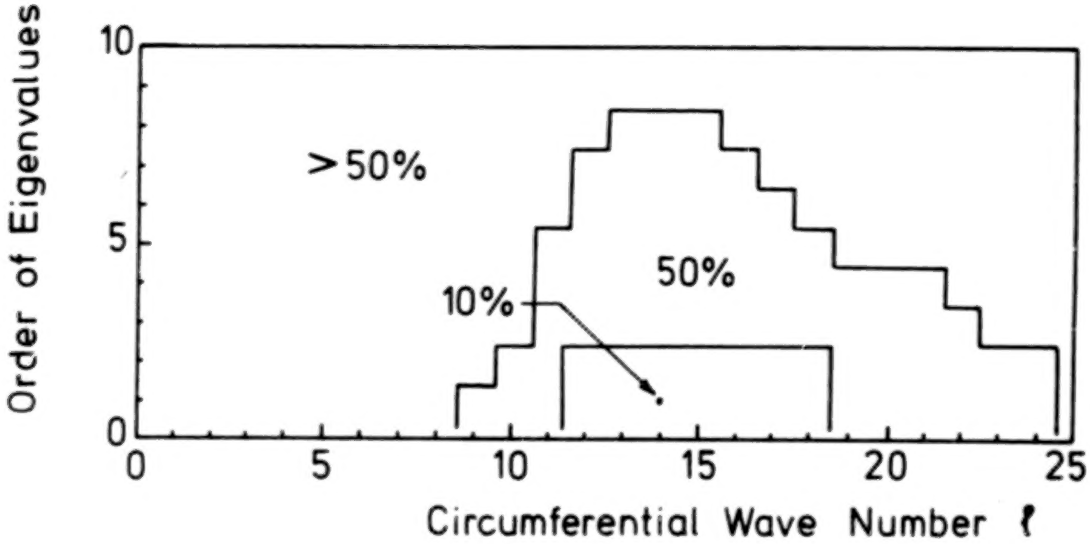

Fig.6 Buckling loads for stringer stiffened shell AS-2
(Boundary conditions : $u = v = w = w_{,x} = 0$).

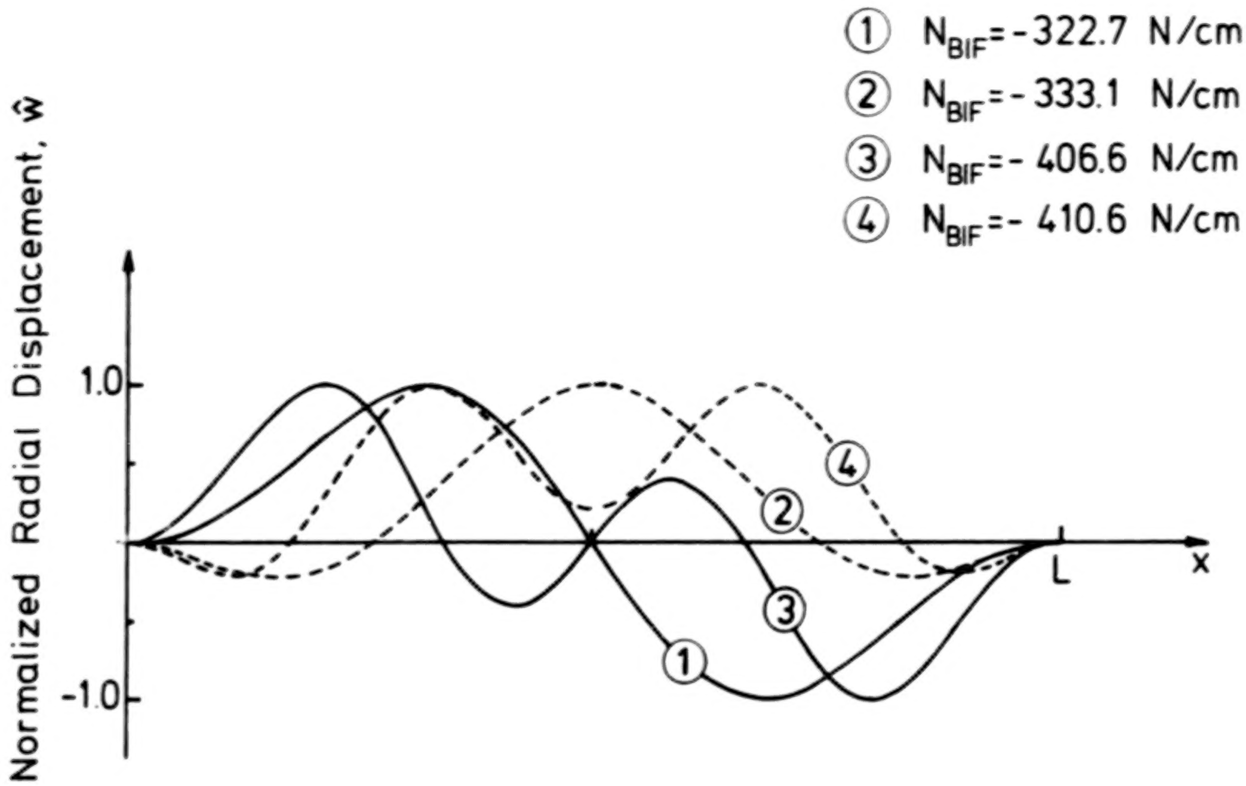

Fig. 7 Buckling modes from linear theory for stringer stiffened shell AS-2 (Boundary conditions: $u = v = w = w_{,x} = 0$; $\ell = 14$).

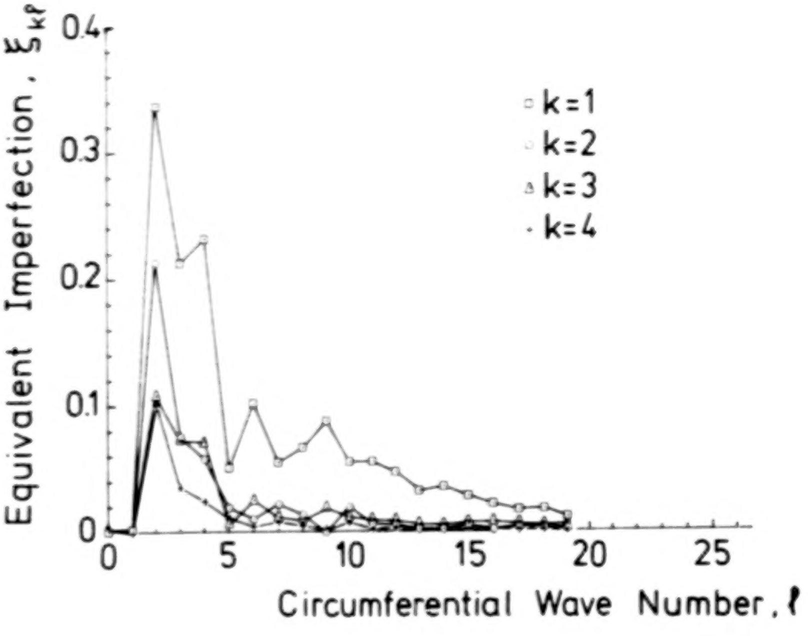

Fig. 8 Circumferential variation of the half-wave sine Fourier representation.

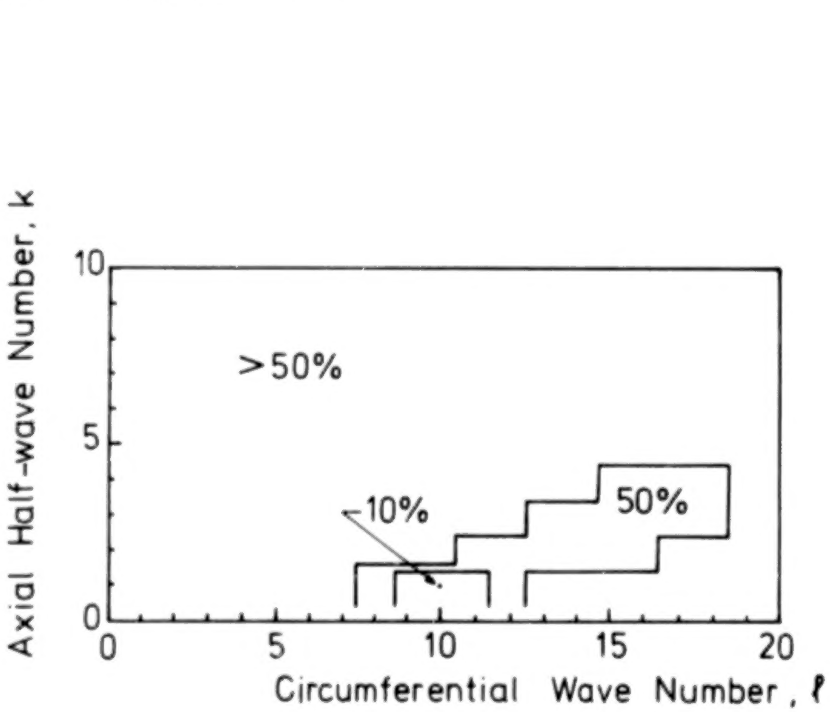

Fig. 9 Buckling loads for stringer stiffened shell AS-2 (Boundary conditions: $N_x = v = w = M_x = 0$).

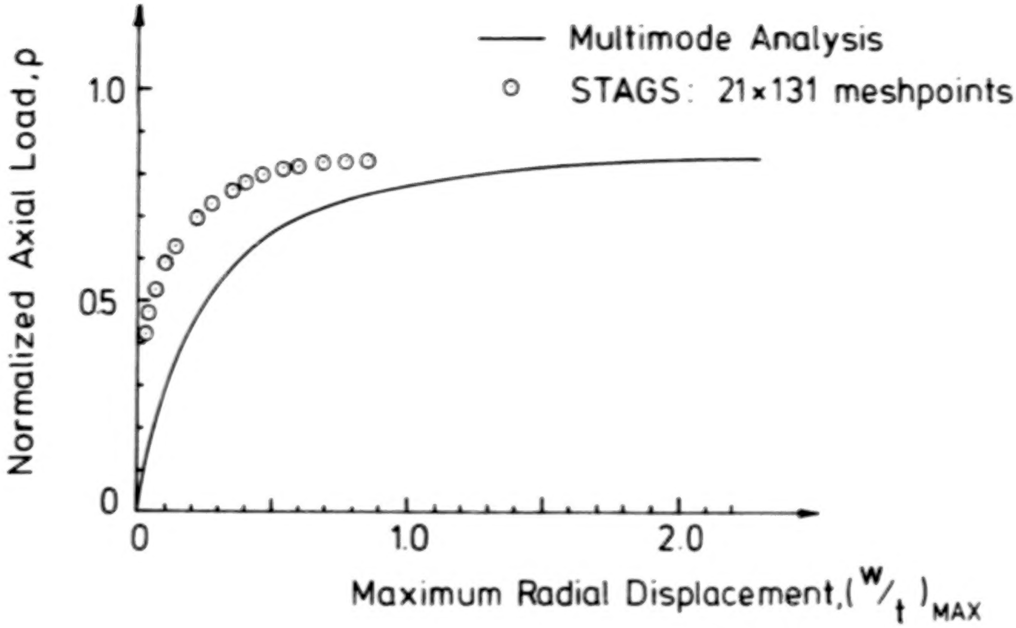

Fig.10 Comparison of Multimode Analysis and STAGS (Shell AS-2, 7-Mode Imperfection Model).

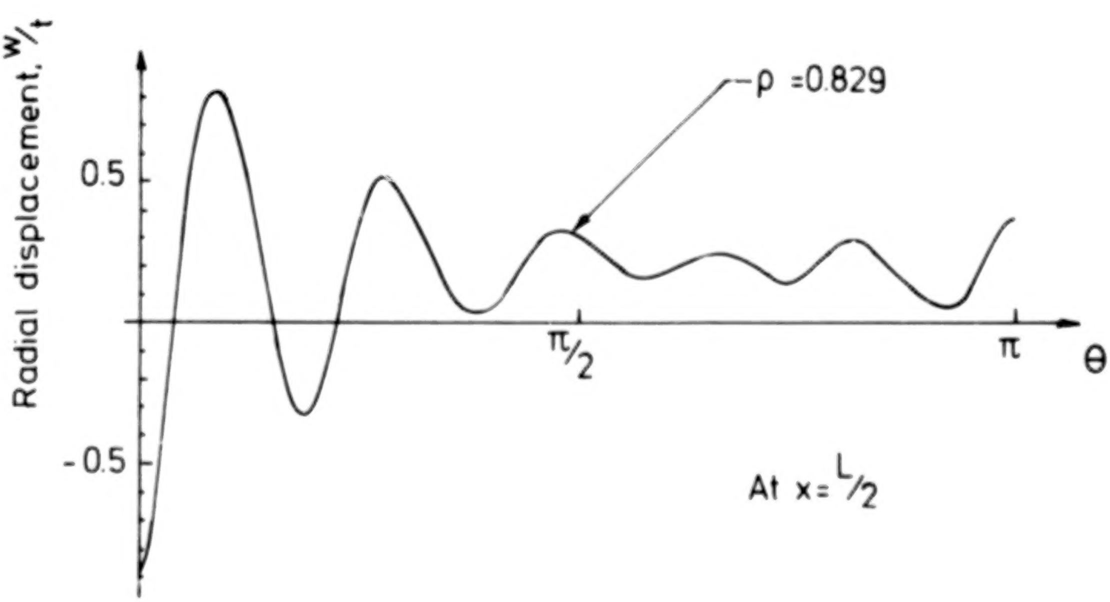

Fig.11 Radial displacement at the limit point by STAGS (Shell AS-2, 7-Mode Imperfection Model).

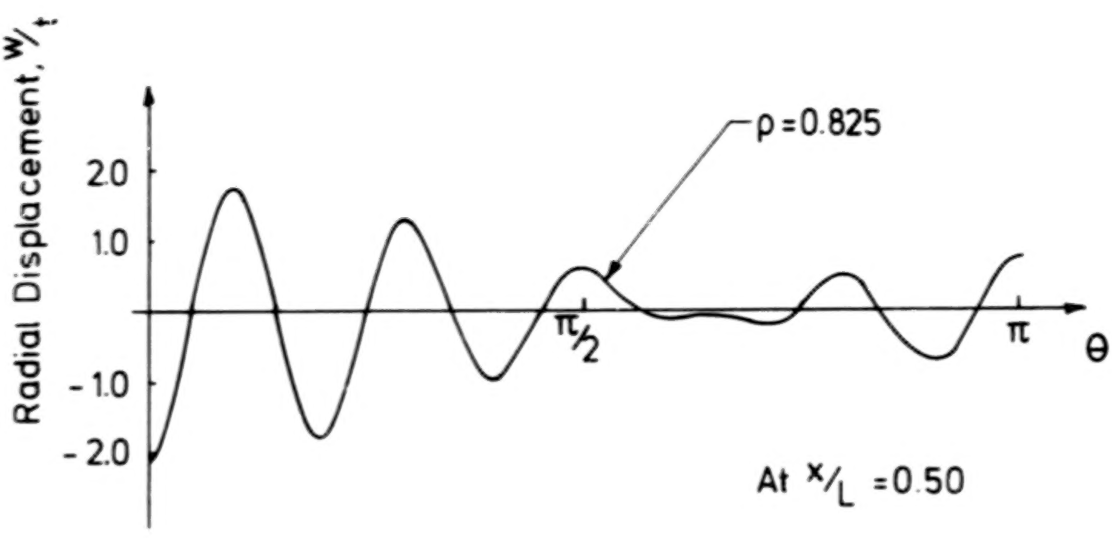

Fig.12 Radial displacement at the limit point by Multimode Analysis (Shell AS-2, 7-Mode Imperfection Model).

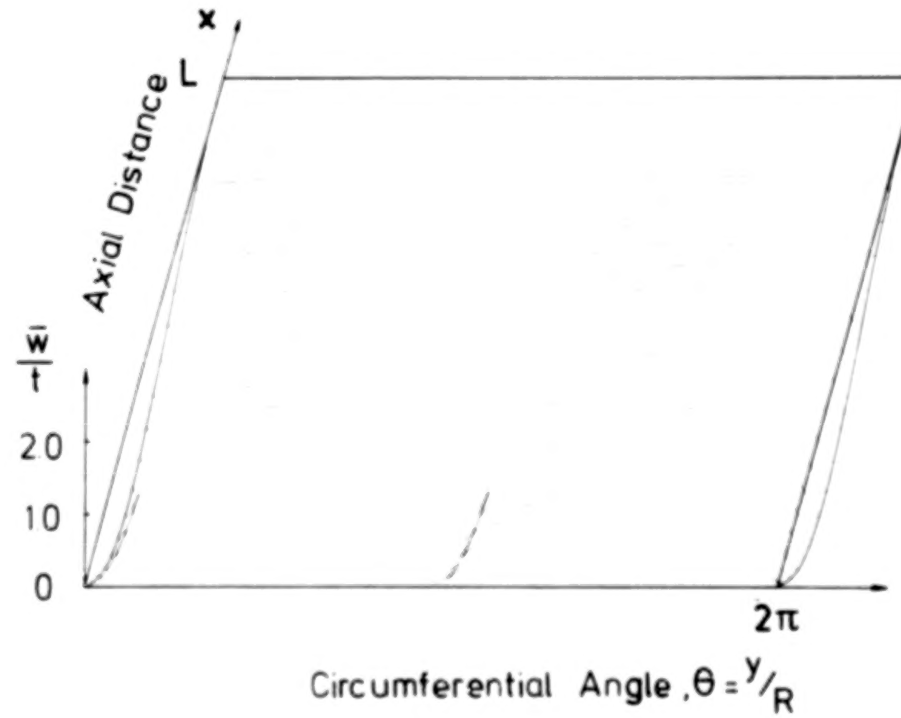

Fig.13 Initial shape of the 30-Mode Imperfection Model.

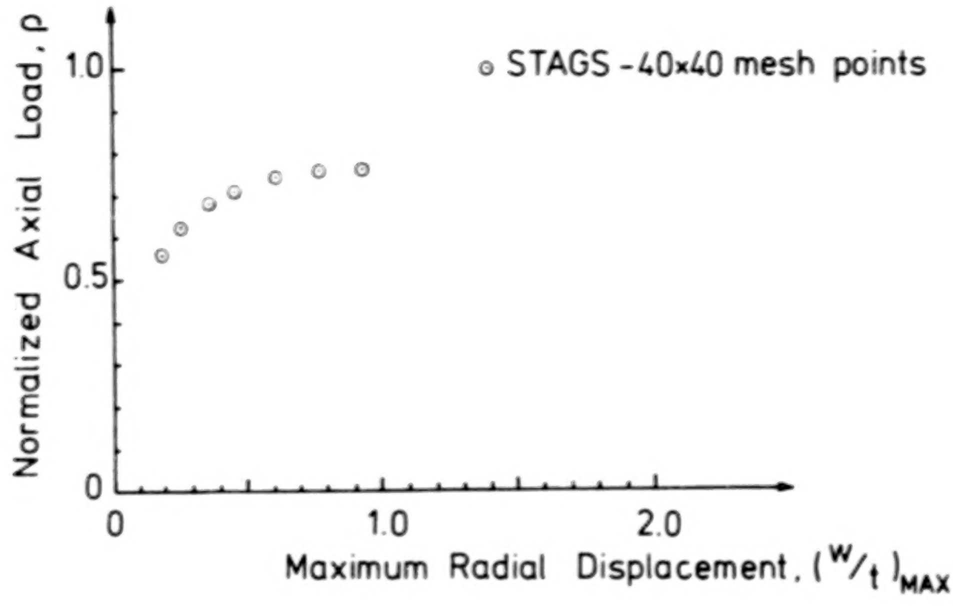

Fig. 14 STAGS Analysis
(Shell AS-2, 30-Mode Imperfection Model).

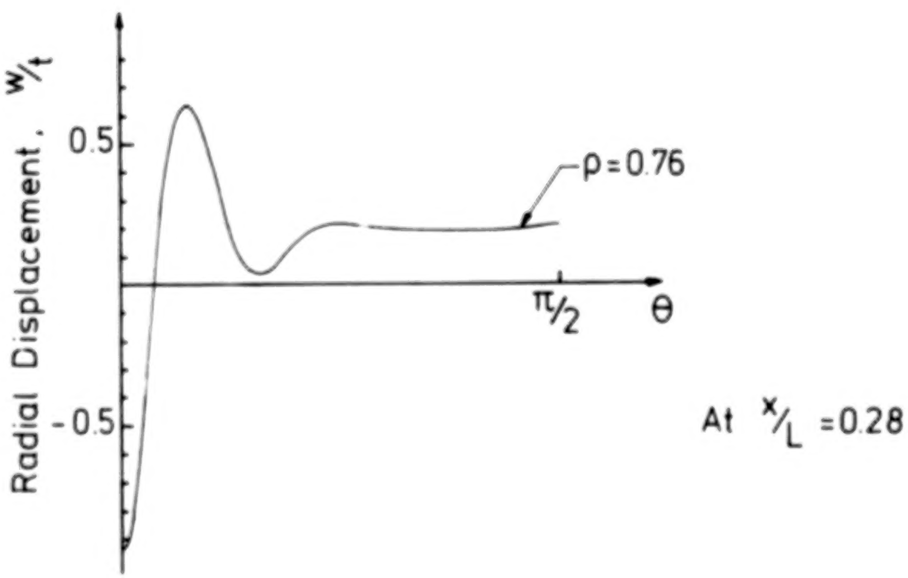

Fig. 15 Radial displacement at the limit point by STAGS
(Shell AS-2, 30-Mode Imperfection Model).

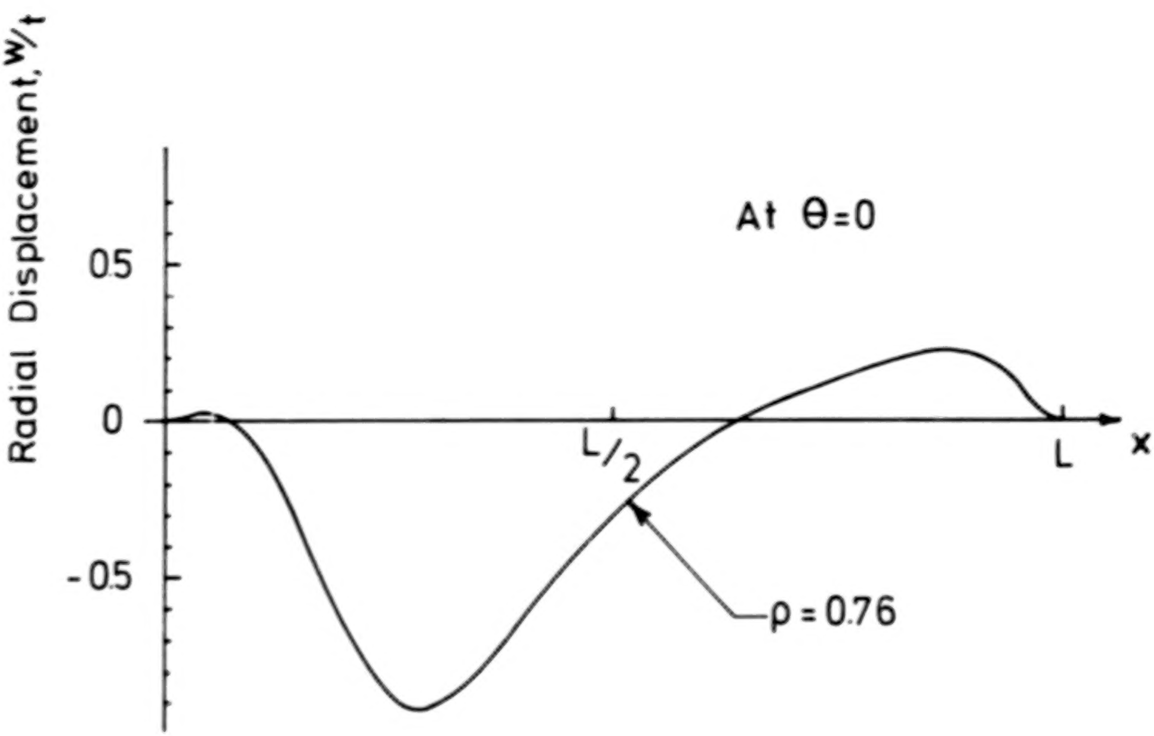

Fig.16 Radial displacement at the limit point by STAGS (Shell AS-2, 30-Mode Imperfection Model).

1. Report No.	2. Government Accession No.	3. Recipient's Catalog No.
NASA CR-3310		

4. Title and Subtitle

The Buckling Analysis of Imperfection Sensitive Shell Structures

5. Report Date

August 1980

6. Performing Organization Code

7. Author(s)

Johann Arbocz and Charles D. Babcock, Jr.

8. Performing Organization Report No.

SM 79-12

9. Performing Organization Name and Address

Graduate Aeronautical Laboratories
California Institute of Technology
Pasadena, CA 91109

10. Work Unit No.

11. Contract or Grant No.

NSG-1005

12. Sponsoring Agency Name and Address

National Aeronautics and Space Administration
Washington, DC 20546

13. Type of Report and Period Covered

Contractor Report

14. Sponsoring Agency Code

15. Supplementary Notes

Langley Technical Monitor: Randall C. Davis
Final Report

16. Abstract

This report describes several types of analyses used to predict the buckling behavior of imperfect shell structures. These analyses are used to study one well characterized stringer-stiffened cylindrical shell. The ability of each analysis to predict the actual experimental buckling load is examined. In addition, the information obtained from each analysis is used when proceeding to a higher level of analysis complexity. Based upon this study, a procedure for calculating a "knockdown" factor is proposed, to replace the traditional empirical knockdown factor.

17. Key Words (Suggested by Author(s))	18. Distribution Statement
Shells, cylinder, imperfections, knockdown factors, stringer stiffeners, analyses, experiments, buckling	Unclassified - Unlimited Subject Category 39

19. Security Classif. (of this report)	20. Security Classif. (of this page)	21. No. of Pages	22. Price
Unclassified	Unclassified	32	A03

For sale by the National Technical Information Service, Springfield, Virginia 22161

NASA-Langley, 1980

31

END

5-22-81